JOURNAL OF OPTOELECTRONICS AND ADVANCED MATERIALS Vol. 8, No. 5, October 2006, p. 1781 - 1795

Feature Paper

Laser remote sensing of tropospheric aerosol

D. NICOLAE*, C. P. CRISTESCU[a]
National Institute of R&D for Optoelectronics, 1 Atomistilor Str., Magurele, Ilfov, Romania
[a] *"Politehnica" University of Bucharest, 313 Splaiul Independentei Str., s. 6, Bucharest, Romania*

Aerosols are one of the greatest sources of uncertainty in climate modeling, by having impact on heat balance of the earth and on clouds properties. The spatial and temporal evolution of the atmospheric aerosol load can be measured effectively by laser remote sensing techniques and in certain conditions their optical and microphysical parameters can be derived. This paper represents an overview of the latest approaches in laser remote sensing, emphasizing on the data processing algorithms and the use of complementary data to overcome non-determination in elastic backscatter Lidar inversion. Original results are also presented.

(Received August 15, 2006; accepted September 13, 2006)

Keywords: Elastic backscatter Lidar, Aerosol optical parameters, Lidar ratio, Inverse problem

1. Introduction

Characterization of the real atmosphere requires a large number of meteorological parameters such as temperature, humidity, wind directions, and in addition, variations in chemical composition and the presence of pollutants, which can undergo rapid local changes, in particular over urban areas. Models of the real atmosphere require many parameters based on a large number of observational data. The design of very accurate models is limited by computer capacity, so in practice simplified models are used. Regardless the complexity of the model, real data are necessary in order to: a) verify, b) validate; c) improve the model.

1.1. Technical background of laser remote sensing

Optical remote sensing techniques are used today for monitoring atmospheric characteristics due to the fact that, conform to the diffraction theory, an obstacle could be "seen" by an electromagnetic wave having a wavelength on the same magnitude as the geometric dimension of the obstacle. So, using a light beam (wavelength nm ... μm) one can detect atmospheric components, which are "invisible" for other sounding waves. The speed of light is also a good argument, because it provides real time response. Another aspect is that a lot of phenomena are produced at the interaction between a light beam and atmospheric constituents, most of these phenomena are specific to the constituent's type. Very important among optical remote sensing techniques are the Lidars based on the use of pulse or continuous lasers as they are characterized by high sensitivity and a long range of penetration. **LIDARs** (**LI**ght **D**etection **A**nd **R**anging) are laser based systems for atmosphere sounding, which allow suspended particulate detection on sounding direction, with a very good precision and in a very short time (seconds). The main components for any Lidar system are the transmitter (pulsed, high power laser), the receiver (telescope + spectrum analyzer + low level, high speed photodetectors) placed on a common platform, and the high speed acquisition system with analog – digital converter. Laser transmitted radiation is scattered by the aerosols, so that a fraction of radiation backscattered by each volume of air can be captured, detected and analyzed. The return signal contains information about the concentration and some physical characteristics of particles in laser beam direction. Lidars are mobile and can thus be used at different sites, including satellites. Lidar measurements permit a highly accurate determination of the type and size of atmospheric components, even at long distances, are able to detect very low concentrations, and allow for a study of their spatial-temporal dynamics.

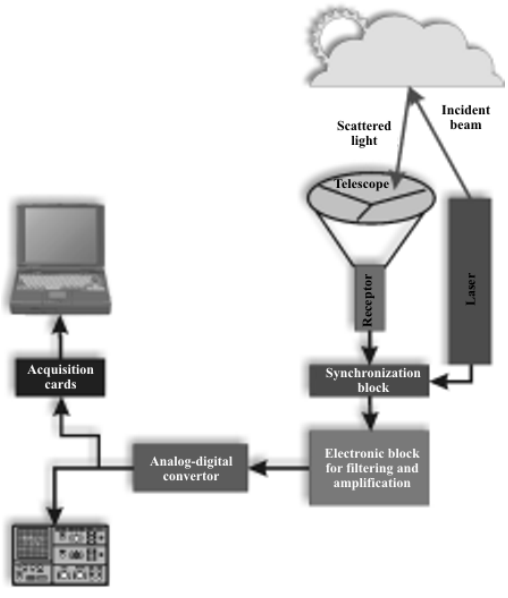

Fig. 1. Lidar principle.

The name "LIDAR" pre-dated the invention of the laser because of other light based techniques using arc-lamp searchlights for atmospheric profiling that started much earlier with Synge (1930) [1], Hulbert (1937) [2], Johnson (1939) [3] and Elterman (1954) [4] using a carbon arc lamp searchlight, followed by Friedland (1956) [5] using a pulsed search light. It's also interesting to note early passive techniques that were developed to profile atmospheric aerosols by observing the sky during sunset.

About the first use of Lidar using a laser, if the definition of Lidar includes hard targets, it was the effort of Smullin and Fiocco in 1962 [6] at Cambridge, where they measured the distance to the moon using a pulsed laser and telescope receiver. Take note of the method of reporting the data. Clearly the invention of the laser was to create many new fields of research since it occurred only two years before these measurements. But if the definition of Lidar requires atmospheric measurements, this effort made by Fiocco and Smullin (1963) [7] is the paper often quoted as presenting the first atmospheric Lidar measurements, which were enabled by the invention of the laser Q-switch, which permits more intense pulses of light energy to be generated by the laser. Fiocco and Smullin describe measurements of atmospheric layers between 60-140 km taken between July 28-31, 1963. Profiles of Rayleigh scattering below the altitude of the "scattering layers" are also shown in this paper.

These measurements sparked considerable interest in other research groups including ones in Jamaica, by Clemesha et. al. [8], where apparently the first depolarization measurements were made of stratospheric aerosols in January 1966, in USA by McCormick et. al. [9] in February 1966 and in England by Bain and Sandford [10], where perhaps the first numerical simulation of Lidar performance is shown based on measurements made in July 1966, and College Park, Maryland, where they describe perhaps the first use of electronic photon counting equipment in Lidar also in October, 1965.

After the development of new lasers and photodetectors in the following years, various types of ground-based Lidar systems (including ceilometers) have been continuously used to probe the earth's atmosphere and to measure a variety of air pollutants, such as O_3, NO_x, SO_2, Hg, toluene, benzene and aerosol optical properties (optical depth, spatial distribution and layering, diurnal variation, etc.), as described by Kölsch (1989) [11], Measures (1992) [12], Bösenberg et al., (2003) [13], Kovalev and Eichinger (2004) [14].

The establishment of the European Aerosol Lidar Network (EARLINET project) on the year 2000 [13], in which INOE Lidar group is an institutional member starting 2005, permitted to establish a 3-years climatology of the vertical distribution of aerosols mainly in central Europe, Greece. Poland and Belarus [13]. During this research, all Lidar systems were inter-compared to prototype-certified Lidar systems both at software and hardware levels [15-17]. Since the beginning of the EARLINET project more than 20000 aerosol vertical profiles under various meteorological conditions, concerning local or long-range transport of aerosols in the free troposphere. including the transport of the Saharan dust towards Europe [18] and Etna volcanic activity in 2005 [19].

In Romania, Lidar activities started in 1993, when a two-wavelength Cu:Br vapors laser based system was build in National Institute of R&D for Optoelectronics INOE, for the detection of aerosol backscattered radiation. For a long period of time this system was used just for air pollution monitoring over a small industrial area in southern Bucharest. Due to the scanty capabilities of the system, no Lidar data where provided until now by Romania, which was not included in EARLINET activities. In the mean time, complementary research like theoretical modeling of the optical field propagation through random and non-homogeneous media [20-22] and statistical automatic data processing for Lidar data validation [23] are also developed. Recently, a new light-weight Lidar was implemented [24,25], in order to extend laser remote sensing applications to in situ tropospheric investigations [26-28], (PBL studies, aerosol density vertical profiles, traffic pollution monitoring). LiSA system is a Nd:YAG laser based Lidar, operating at 1064 and 532 nm wavelengths, providing in real time aerosol density profiles up to 10 Km high, with a 6 m spatial resolution. Its compact design and cinematic characteristics allows field implementation and large areas surveillance.

1.2. Theoretical background of atmosphere investigation by Lidar

The description of the laser beam interaction with atmospheric constituents (i.e. molecules, particles, clouds) is based on the fundamental theory of electromagnetic wave propagation in various media, well represented in the scientific literature [29-35].

But in fact, one must consider for the theoretical approach that the atmosphere contains a wide range of constituents extending from atoms and molecules (Angstrom range d ~ 10^{-3}-10^{-4} μm) to aerosols (d ~10^{-2}-5 μm), cloud water droplets and ice crystals (d ~1 –15 μm and even larger). In the last decades, atmospheric composition and properties were studied by various laboratory or in situ techniques in different meteorological conditions and for different classifications [36-64]. From the laser remote sensing point of view, the basic information that can be used from these studies is that the mixture of these different components results in a series of complex atmospheric interactions that take place with a laser beam. All these phenomena can be used to derive information about the atmosphere. For that, the set-up of the system is different according to the selected phenomena. In all cases, the intensity of the light resulting from these processes is proportional with the initial intensity I_0, the number density of the active diffusers n and the differential angular cross – section σ [65] and this can be used to derive some optical / microphysical parameters of the diffusers in the beam path.

The molecular and aerosol elastic/inelastic processes involved in the use of the Lidar method for atmospheric investigations are the following [12]:

(a) N_2, O_2 molecular elastic ($\lambda_D = \lambda_L$) light scattering; i.e. Rayleigh diffusion ($\lambda_L >> d$, where d is the molecular diameter)

(b) Aerosol elastic ($\lambda_D = \lambda_L$) light scattering; i.e. Mie scattering ($\lambda_L \sim d$, where d is the diameter of the particle)

(c) N_2, O_2 and H_2O molecular inelastic ($\lambda_D \neq \lambda_R$) light scattering; i.e. Raman scattering ($\lambda_L >> d$, with d the molecular dimension)

(d) Gas and aerosol absorption (if the radiation at λ_L is absorbed by atmospheric molecules or by compounds forming the aerosols)

(e) Fluorescence of bioaerosols

As previous mentioned, everyone of these processes can give information about a certain atmospheric component. Due to their large influence on earth's radiation budget [66], aerosols are an important factor to be studied, especially because of their variability in time and space. For example, tropospheric aerosols arise from both natural sources (wind-borne dust, volcanic eruptions, etc.) and anthropogenic activities (fossil fuels combustion, biomass burning activities, industrial activities, etc.) [67]. As a consequence, their composition is highly variable [68-70]. Atmospheric particles play an important role in earth's radiation budget and climate, by scattering and absorbing both incoming and outgoing radiation depending on their chemical composition [71,72]. However this role has not been precisely estimated yet [73] and needs future investigations.

Recent estimations on the possible impact of aerosols (both direct and indirect effects) on the radiative forcing (cooling effect) in a global average are of the same order of magnitude as the CO_2 effect (warming effect). However, high uncertainties still exist concerning the indirect and direct effects, which are connected with the aerosol influence on climate. By employing several wavelengths [74] the Lidar provides very accurate information about the size distribution of aerosol particles as well as their concentrations under various weather conditions and at different altitudes above sea level.

The variable gases present themselves as interesting components of the atmosphere to study using Lidar due to their highly variable structure and the importance of understanding atmospheric processes relating to their production or destruction (e.g.chloro-fluorocarbons and ozone in the stratosphere).

Differential Absorption Lidar (DIAL) is useful for studying various gases in the atmosphere using tunable lasers. Raman Lidar is also useful in this respect since with a single laser Raman lines can be excited from a variety of molecules.

The use of Raman Lidar for profiling water vapor mixing ratio in the atmosphere is a well-established experimental technique.

2. Aerosol monitoring by elastic backscatter Lidar

Due to its relative low cost, high reliability and easy operation, the backscatter Lidar is common used for aerosol and clouds study. It measures the backscattering at the laser wavelength due to molecules (Rayleigh scattering) and particles (Mie scattering). Both co-axial and bi-axial configurations can be used. In order to filter the unwanted radiation (in this case the only useful wavelength is the wavelength of the laser) an interference filter is placed in front of the photodetector. For different laser wavelength (IR, VIS or UV), the photodetectors can be PMT or APD, but anyway they must be fast, sensitive and low noise. Fast detectors give a good spatial resolution, sensitive detectors allow to detect low concentrations, low noise detectors allow to extend the maximum range as far as possible (troposphere, even stratosphere!). The acquisition system must also be fast. In order to obtain a significant Signal to Noise Ratio (>10), two type of detection are used: analog detection for lower part of the signal (PBL) and photon counting for the upper part, where the atmospheric noise superimposed on the signal is much higher. If the Lidar is designed to measure beyond the PBL, then both methods must be used simultaneously and the 2 signals must be glued into one profile.

2.1. Molecular (Rayleigh) scattering

In the case of the molecular scattering [75], the atmospheric molecules scatter the incident radiation elastically. If the excitation wavelength is much higher than the dimension of the atoms and molecules, the Rayleigh scattering condition is fulfilled.

The Rayleigh backscattering is proportional to the diffusers' number density and to the Rayleigh differential cross section. The air differential (angular) Rayleigh cross-section, $d\sigma_m/d\Omega$ (cm^2 $molecule^{-1}sr^{-1}$), may be expressed as:

$$\frac{d\sigma_m(\phi,\theta,\lambda)}{d\Omega} = \frac{9\pi^2\left(m_{air}^2-1\right)^2}{\lambda^4 n_{air}^2\left(m_{air}^2+2\right)^2}\cdot\left(\frac{6+3\rho}{6-7\rho}\right)\cdot\left\{\cos^2\phi\cos^2\theta+\sin^2\phi\right\} \tag{1}$$

For the backscattering:

$$\sigma_m(\lambda) = \frac{8\pi}{3}{}^{\pi}\sigma_m(\lambda) \tag{2}$$

and the molecular extinction coefficient α_m (Z) and the backscattering coefficient β_m (Z)can be obtained:

$$\alpha_m(Z) = \frac{8\pi}{3}\beta_m(Z) = \frac{8\pi}{3}n_{air}(Z)\frac{{}^{\pi}d\sigma_m}{d\Omega} \tag{3}$$

with α_m expressed in m^{-1} and β_m in $m^{-1}sr^{-1}$. The air number density n_{air} (Z) is determined from the air pressure and temperature profiles as measured by radiosondes or estimated using atmospheric models. The formula above

indicates a Rayleigh cross-section that follows a ~ λ^{-4} wavelength dependency, and for this reason, the shorter the wavelength, the more scattered the corresponding radiations. The scattering cross-section is relatively small, on the order of ~ 10^{-28} cm^2/molec, but the air concentration number i.e. ~ 10^{19} molec/cm^3 partially compensates for the inefficiency of this process.

2.2. Aerosol (Mie) scattering

In the presence of particles of size comparable to the excitation wavelength (> 0.1 μm), Mie scattering processes becomes important [29]. Thus the laser radiation is elastically scattered ($\lambda_D = \lambda_L$) by small atmospheric particles (i.e. aerosols) of size comparable to the radiation wavelength. The Mie backscatter usually dominates the Rayleigh scattering, exhibiting high cross-section values ranging from 10^{-26} to 10^{-8} cm^2/molec (e.g. 10^{-10} cm^{2}molec^{-1} in the visible spectra at ~500 nm for particles with size around 0.1 μm).

The angular characteristics of Mie scattering (i.e. cross-section) for all particle sizes and wavelengths are expressed by two intensity distribution functions. These functions are fundamental for all the subsequent definitions of the scattering cross sections and volume coefficients:

$$i_c(\chi,m,\theta)=\left[\sum_{n=1}^{\infty}\frac{2n+1}{n(n+1)}\left(a_n\pi_n+b_n\tau_n\right)\right]^2$$
$$i_p(\chi,m,\theta)=\left[\sum_{n=1}^{\infty}\frac{2n+1}{n(n+1)}\left(a_n\tau_n+b_n\pi_n\right)\right]^2 \quad (4)$$

where n are positive integers. The values of a_n and b_n result from Ricatti-Bessel functions, the arguments of which are the size parameter χ, and the complex refractive index, m. The functions π_n and τ_n depend only on the angle θ and involve the first and second derivatives of the Legendre polynomials of order n and argument $cos(\theta)$.

The intensity of the light scattered by the particles is:

$$I(\theta,\phi)=E_\phi\frac{\lambda^2}{4\pi^2}\left(i_c\sin^2\phi+i_p\cos^2\phi\right) \quad (5)$$

where E_φ is the irradiance of the incident light and it can be seen that this time the diagram is not symmetric.
The differential cross-section $d\sigma/d\Omega$ [cm^2/sr/molec] is given by:

$$\frac{d\sigma_a(\theta,\phi)}{d\Omega}=\frac{I(\theta,\phi)}{E_\phi}=\frac{\lambda^2}{4\pi^2}\left(i_c\sin^2\phi+i_p\cos^{2\phi}\right) \quad (6)$$

An important optical parameter for the atmosphere is the asymmetry parameter:

$$\frac{d\sigma_a(\theta,\phi)}{d\Omega}=\frac{I(\theta,\phi)}{E_\phi}=\frac{\lambda^2}{4\pi^2}\left(i_c\sin^2\phi+i_p\cos^{2\phi}\right)$$
$$g=\frac{\int_0^\pi\sigma_a(\theta)\cos(\theta)\sin(\theta)d\theta}{\int_0^\pi\sigma_a(\theta)\sin(\theta)d\theta} \quad (7)$$

For isotropic or symmetric scattering (e.g. Rayleigh or spherical particle scattering), the asymmetry parameter is zero, while for a purely forward scattering the parameter is 1. The asymmetry parameter of the cloudless atmosphere ranges from 0.1 (very clean) to 0.75 (polluted). For a cloudy atmosphere, asymmetry parameter values vary between 0.8 and 0.9 [80]. The total scattering cross section σ_a [cm^2/molec] may be calculated by integrating over the 4π sr

$$\sigma_a=\int_0^{4\pi}\frac{d\sigma_a(\theta,\iota)}{d\Omega}d\omega=2\pi\int_0^\pi\sigma_a(\theta)\sin(\theta)d\theta \quad (8)$$

The ratio of the scattering to geometric cross sections is defined as the efficiency factors as follows:

$$Q_{scat}=\frac{\sigma_a}{\pi r^2}=\frac{2}{r^2}\int_0^\pi\sigma_a(\theta)d\theta\,;Q_\pi=\frac{\sigma_a(\theta=\pi)}{\pi r^2} \quad (9)$$

where r is the radius of the aerosol particle and the complex part of the refractive index is not taken into account. The link between the extinction α, backscatter β coefficients and the efficiency factors Q_{scat} and Q_π is given by

$$\alpha_a=\pi\int_0^\infty r^2Q_{ext}\,n(r)dr\;;$$
$$\beta_a=\pi\int_0^\infty r^2Q_\pi n(r)dr \quad (10)$$

where $n(r)$ is the aerosol size distribution and in the calculation of Q_{ext} the complex part of the refractive index is taken into account (i.e. $Q_{ext} = Q_{scat} + Q_{abs}$). The ratio of the scattering (Q_{scat}) to extinction efficiency factors is called single scattering albedo (ω_0), which represents the fraction of scattered light with respect to the total light. For a non-absorbing particle, the single scattering albedo is 1.

2.3. Lidar equation and inversion algorithm

The magnitude of the received Lidar signal is proportional to the number density of the atmospheric diffusers (molecules or aerosols), their intrinsic properties (i.e. probability of interaction with the electromagnetic radiation at the laser wavelengths, called cross–section value) and with the laser incident energy. The detected light backscatter power $S(Z, \lambda)$ at the wavelength λ from a distance Z can be expressed by the so-called Lidar equation as follows [76]:

$$S(\lambda_D,Z)=S(\lambda_L,Z_0)\cdot K_S(Z)\frac{A_0}{Z^2}\delta Z\cdot\beta_{atm}(\lambda_D,\lambda_L,Z)\cdot T_{\rightarrow}(\lambda_L,Z)\cdot T_{\leftarrow}(\lambda_D,Z) \quad (11)$$

where $S_L(\lambda_L,Z_0)$ represents the mean power emitted by the laser source at wavelength . The λ_D is λ_L the wavelength at which the backscattered radiation is detected by the Lidar receiver. The radiation is usually detected at the laser wavelength (λ_L, elastic processes) but the shifted in wavelength radiation due to inelastic processes as the Raman effect may be also detected. K_S *(Z)* is the instrument function that takes into account the transmitter and receiver efficiencies, the overlap function (the degree of spatial recovering between the emitted beam and the receiver field of view). A_0 is the effective receiver area (i.e. area of the telescope collector mirror) and δZ is the spatial resolution.

$T_{\rightarrow}$ is the atmospheric transmittance from the transmitter to the probed volume and $T_{\leftarrow}$ is the atmospheric transmittance from the probed volume to the receiver, and they are calculated as follows:

$$T_{\rightarrow}(\lambda_L,Z)=\exp\left[-\int_{Z_0}^{Z}\alpha_{atm}(\lambda_L,z)dz\right];$$
$$T_{\leftarrow}(\lambda_D,Z)=\exp\left[-\int_{Z}^{Z_0}\alpha_{atm}(\lambda_D,z)dz\right] \quad (12)$$

where α_{atm} *(λ, Z)* is the atmospheric extinction coefficient and may be different on the two directions of the laser pulses, as is the case of the Raman backscatter radiation ($\lambda_R \neq \lambda_L$). The atmospheric backscattering coefficient, β_{atm} *(λ, Z)*, is a key element of the Lidar equation Eq. (1), and is proportional to the cross-section of the involved physical process σ_{atm} (λ_L,λ_D, *Z*) and to the number density *n (Z)* of the atmospheric active diffusers (i.e. atoms, molecules, particles, clouds) in the probe d volume. The subscript "*atm*" encompasses all possible physical interactions within the atmosphere.

Another often-used form of the Lidar equation is

$$RCS(\lambda_D,Z)=C_S(Z)\cdot\beta_{atm}(\lambda_D,\lambda_L,Z)\cdot T_{\rightarrow}(\lambda_L,Z)\cdot T_{\leftarrow}(\lambda_D,Z) \quad (13)$$

where *RCS* is the range corrected signal

$$RCS(\lambda,Z)=S(\lambda,Z)\cdot Z^2 \quad (14)$$

and *Cs (Z)* is the instrument function.

When the Lidar equation is adapted to the specific process involved (i.e. Rayleigh, Mie, Raman), various atmospheric properties and parameters can be retrieved. An ideal Lidar that can explore all these processes is obviously a multiwavelength system, but this is generally too expensive and difficult to operate.

The elastic backscatter signals (i.e.$\lambda_D = \lambda_L$) are due both to the molecular (i.e. Rayleigh scattering) and to aerosols/clouds (i.e. Mie scattering) backscatters. The backscattered light is proportional to the number density of diffusers (i.e. molecules and aerosols) and to the volume backscattering cross-sections of Rayleigh and Mie processes. The Lidar-detected range corrected signals *RCS(Z)* at λ_L may be written as follows:

$$RCS(\lambda_L,Z)=C_S(\lambda_L,Z)\cdot\beta_t(\lambda_L,Z)\cdot\exp\left[-2\int_0^Z\alpha_t(\lambda_L,z)dz\right]+b(\lambda_L,Z) \quad (15)$$

where λ_L is the laser emitted – detected wavelength (i.e. λ_L = 355, 532 and 1064 nm), C_S is a system function, β_t is the total backscattering coefficient, α_t is the total extinction coefficient and *b* is the background signal (electronic, solar-moon induced noise, light contamination sources, homogeneous or shaped offsets of the detector's base line, etc). The β_t [$m^{-1}sr^{-1}$] and α_t [m^{-1}] coefficients may be expressed as the sum of the aerosols (a) and molecular (m) contributions:

$$\beta_t(\lambda_L,Z)=\beta_a(\lambda_L,Z)+\beta_m(\lambda_L,Z)+\beta_{tracegases}(\lambda_L,Z)$$
$$\alpha_t(\lambda_L,Z)=\alpha_a(\lambda_L,Z)+\alpha_m(\lambda_L,Z)+\alpha_{abs}(\lambda_L,Z) \quad (16)$$

The effect of tracegases and absorption will be neglected due to the very weak contribution of backscatter and absorption of trace gases at the Lidar wavelengths. The molecular contribution β_m and α_m may be estimated taking into account the Rayleigh scattering theory.

To analyze the return signal in laser remote sensing means to find solutions for the equation which relates the characteristics of the received and emitted signal, and the propagation medium. The form of the equation depends of the interaction type, as we mentioned before.

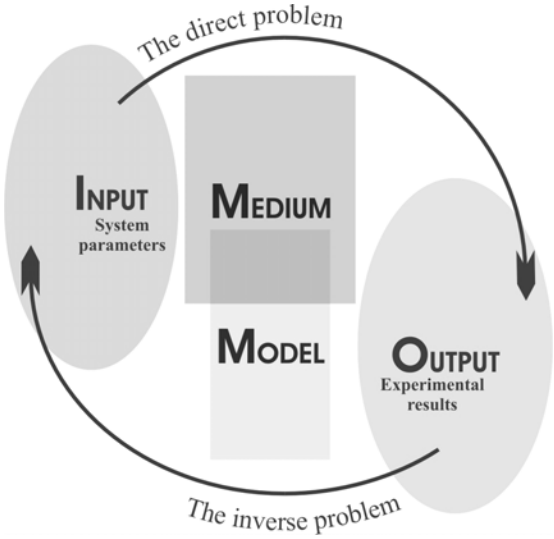

Fig. 2. The direct and inverse problem in Lidar sounding.

For the inversion of the backscatter Lidar equation the Fernald-Klett method is used [77,78]. It must be underlined that in this case we have 2 unknown parameters (backscattering and extinction coefficients) and only one equation! Also, to obtain the solution we have to integrate, so the limit conditions must be given.

For that, two a priori assumptions are necessary to allow the retrieval of $\alpha_a(Z)$ and $\beta_a(Z)$ profiles:

(i) the guess of the aerosol Lidar ratio (LR_a) value (extinction/backscattering)

$$LR_a(Z)=\frac{\alpha_a(Z)}{\beta_a(Z)} \tag{17}$$

(ii) a known reference value at a given altitude (e.g. a region with a molecular value): $\beta_a(Z_c)$

With these assumptions, the Fernald-Klett solution of the backscatter Lidar equation can be written:

$$\beta(Z)=-\beta_m(Z)+RCS(Z)\cdot\exp\left[-2(LR_a(Z)-LR_m)\cdot\int_{Z_C}^{Z}\beta_m(z)dz\right]\cdot \left[\frac{RCS(Z_C)}{(\beta_a(Z_C)+\beta_m(Z_C))}-2LR_a(Z)\int_{Z_C}^{Z}RCS(z)\cdot\exp\left[-2(LR_a(z)-LR_m)\cdot\int_{Z_C}^{Z}\beta_m(z')dz'\right]dz\right]^{-1} \tag{18}$$

where LR_m is the molecular Lidar ratio and has a constant value of $8\pi/3$.

All molecular parameters can be calculated with sufficient accuracy from ground values of pressure and temperature using atmospheric model [79], for the reference value of backscattering coefficient a molecular assumed value at high altitude can be considered, but for solving the equation for the aerosol backscatter, the Lidar ratio profile must be evaluated. LR_a depends on the aerosol microphysics and can vary between less than 10 sr (ice crystals) and more than 100 sr (heavily polluted air) [80]. It depends on humidity and aerosol mixture and therefore, on height. One possibility is to measure LR_a using either high spectral resolution Lidar [81,82], either Raman Lidar [83]. But even so, LR_a can only be measured for the lowest part of the profile, where the Raman signal is strong enough, and only when the background radiation is small enough to have a significant signal to noise ratio (nighttime generally). For this reason, additional methods to eliminate non determination in Lidar equation were developed.

2.4. Optical parameters extracted from Lidar signal

The detected signal of the Lidar system is the result of the molecular and aerosol scattering. So, the parameters to be derived are the backscattering coefficient and the extinction coefficient. These are optical parameters. Other optical parameters can be derived too if the system is complex enough (multi-wavelength for example) [80]:

1) Angstrom coefficients *A, B* - that describe the wavelength dependency of the extinction coefficient:

$$\alpha_a=B\lambda^{-A} \tag{19}$$

2) Depolarization ratio $\varphi(Z)$ - is calculated as the ratio of cross (c) to parallel (p) polarization states of the backscatter radiation relative to the initial linear polarization plan of the emitted laser light

$$\varphi_{atm}(Z)=C_S(Z)\frac{S_c(Z)}{S_p(Z)} \tag{20}$$

where *Cs* is a calibration function taking into account the whole system depolarization effects. The depolarization ratio may be used to distinguish between spherical (e.g. water droplets, with low depolarization ratios) or nonspherical (e.g. ice crystals, with high depolarization ratios). It can be also indirectly an indicator about the hydration rate (humid or dry) of aerosols or even about their lifetime (aged or fresh) and their physical composition (water or ice content).

3) Aerosols' optical depth or thickness (*AOD* or *AOT*) - is the extinction coefficient integrated on an atmosphere path cf. Eq. (1) generally scaled at the zenith direction.

$$AOD=\int_{Z_0}^{Z}\alpha_a(z)dz \tag{21}$$

4) Aerosols single-scattering albedo - is the scattering to extinction ratio

$$\omega_0=\frac{Q_{scat}}{Q_{ext}} \tag{22}$$

More then optical, microphysical parameters of aerosols can be derived by processing Lidar data (some additional information are still required) [80]:

1) Surface-area weighted effective radius r_e

$$r_e(Z)=\frac{\int n(r,Z)r^3dr}{\int n(r,Z)r^2dr} \tag{23}$$

2) Total surface-area concentration a_t [μm^2cm^{-3}], the total volume concentration v_t [μm^3cm^{-3}], and the total number concentration n_t of particles [cm^{-3}]

$$\begin{aligned} a_t&=4\pi\int n(r)r^2dr\\ v_t&=\frac{4\pi}{3}\int n(r)r^3dr\\ n_t&=\int n(r)dr \end{aligned} \tag{24}$$

3) The complex refractive index of aerosols

$$m(RH)=n(RH)-i\cdot k(RH) \tag{25}$$

where

$$\begin{cases} n(RH)=n_W+(n_0-n_W)\left(\frac{r_0}{r}\right)^3\\ k(RH)=k_W+(k_0-k_W)\left(\frac{r_0}{r}\right)^3 \end{cases} \tag{26}$$

All these parameters can be derived from Lidar data with sufficient accuracy if:

- the system provides reliable data (good alignments, high stability)
- the algorithm for data processing is optimized (some preliminary data and approximations must be considered, based on other sources - point monitors, radiosondes, models ...)

3. Experiments

3.1. Lidar system in Bucharest

LiSA (Lidar for Sounding the Atmosphere) at the National Institute of R&D for Optoelectronics is an elastic backscattering Lidar which can detect from distance (max. 10 Km) micronic aerosols, with a spatial resolution of 6 m, using as sounding radiation the beam of a laser which works on two wavelengths: 532 and 1064 nm [84].

The main component of the emission block is a pulsed, Q-switched YAG:Nd laser, which produces short pulses (6 ns length) in a beam with 0.5 mrad divergence. A part of emitted laser pulse is utilized as marker of 'zero' time (the reference signal to normalize the return signal, when the reproductibility of laser emission is not proper). The backscattered field collected by the receiver optics is passed through a spectrum analyzer, which selects only the specific wavelength interval of interest for the application, in order to minimize the background radiation contribution. The electric signal generated by photodetectors is electronically synchronized, amplified and converted in digital signal, which is finally delivered to a PC for processing.

The main characteristics of LiSA system are:

Emitter Nd:YAG laser LS-2131	
Working wavelengths	1064, 532 nm
Pulse energy at 1064 nm	100 mJ
Pulse energy at 532 nm	50 mJ
Pulse repetition rate	20 Hz
Pulse duration (at level 0.5)	10-12 ns
Angular beam divergence (at level 0.5)	1.5 mrad
Telescope's main mirror diameter	260 mm
Field of view	2.5 - 18 angle min
Focal length	1054 mm
Halfwidth of the interference filters	2.5 nm
Digit capacity of ADC	12 bit
Sampling frequency of ADC	25 MHz

LiSA system was placed in a special laboratory, in Magurele city, located at a proper height in order to permit near-horizontal sounding too, towards Bucharest limits. This location put some problems related to optimal choosing of the calibration point so that the information obtained from signal inversion to be trustable [85]. Magurele Platform, where the system is placed, is about 5 Km away from Bucharest and is separated from it by much less populous zone, much less polluted in consequence. Most important contribution to the backscattering signal comes from the aerosols over the city, but the contribution of Magurele sources cannot be neglected, having in view that even here there is some industrial activity and traffic. For this reason, the calibration point cannot be selected at the end of the sounding path, where the atmospheric extinction coefficient is very high due to the city. But neither can be selected at the beginning of the path because – by the forward integration – the solution of Lidar equation become unstable. The calibration point must be selected between the 2 limits, as possible in the area where the atmospheric extinction coefficient is smallest, but in our case this area is dependent of weather and time of the day. These problems are specific for slanting sounding. For vertical sounding the situation is much simple because it is known that over the Planetary Boundary Layer (PBL), in free troposphere, the value of the extinction coefficient is minimal, and this particular height can be selected as calibration point.

3.2. Methodology

In order to increase the spatial resolution of the Lidar system, a new acquisition card (100 MHz) was used. Also, the control and measurement software was upgraded in order to provide 3 hours automatic measurements with a 3 m spatial resolution and 1 min temporal resolution. The experiments were done during several days at various hours, daytime and nighttime, to study both PBL height variations and aerosols vertical distribution [86]. In order to derive aerosols optical parameters and Lidar ratio from elastic backscatter Lidar data a dedicated LabVIEW program was developed on the basis of a special iterative algorithm.

LiSA system signal processing method is based on Fernald-Klett combined, with atmospheric model and Mie algorithm for direct problem (theoretical calculation of optical parameters), all integrated in an iterative program to identify the proportions of aerosol components for which the best fit between theoretical and retrieved optical parameters is achieved [87]. The altitude profile of molecular extinction coefficient $\alpha_m(Z)$ is calculated from pressure and temperature profiles (using either radiosondes data, either atmospheric model) 0.

$$\alpha_m(h;p,T)=\frac{24\pi^3\left(m_{aer}{}^2-1\right)^2}{\lambda^4 N_s{}^2\left(m_{aer}{}^2+2\right)^2}\cdot\frac{6+3\gamma}{6-7\gamma}\cdot N_s\frac{T_0}{p_0}\cdot\frac{p(h)}{T(h)} \quad (27)$$

where $m_{aer}=$ is the refractive index of air, γ is the depolarization factor (0.0284 for $\lambda=532$ nm, 0.0273 for $\lambda=1064$ nm respectively), and $N_s=2.547\times10^{19}$ cm^{-3} is the molecular number density for standard atmospheric conditions at ground level ($p_0=1013.25$ hPa, $T_0=15$ ^{o}C).

In order to overcome the nondetermination in Lidar equation and the lack of direct Lidar ratio measurements, the processing algorithm must be improved by using complementary data, such as those provided by the Ackermann model [88]

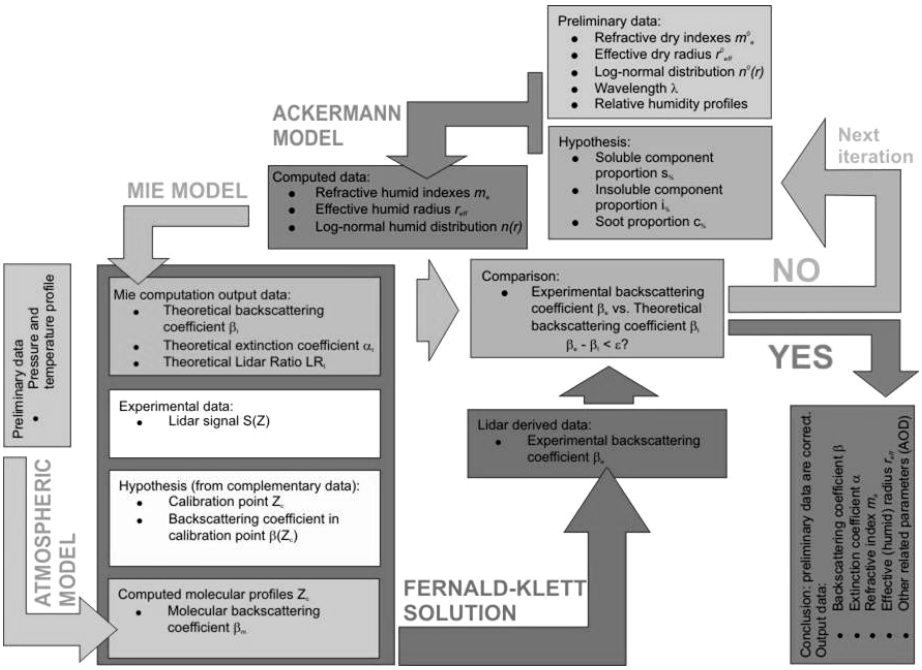

Fig. 3. Schematics of LiSA hybrid algorithm.

In our algorithm, it is assumed that the aerosol is an external mixture of internally mixed components. Each aerosol component (indexes *s,i,c*) is lognormally distributed with respect to the particle radius and representative to tropospheric continental aerosol type. Therefore we consider 3 types aerosol particles 0: soluble(s), insoluble (i) and carbonic components (c) characterized by the number mixing ratio μ:

$$\mu_s + \mu_i + \mu_c = 1 \tag{28}$$

For given optical properties and a distinct relative humidity *RH*, the variability of the Lidar ratio is caused by different number mixing ratios μ_k. The water soluble component is the only component whose properties are affected by the relative humidity. The mixing ratio μ_s can be varied between 0.1 and 1 in steps of 0.1. Accordingly, since μ_i is about four orders less, μ_c, chosen to be the controlling parameter in our algorithm, is iterated in 0.01 steps from 0.1 to 1.

On each iteration we calculate humid log normal distribution parameters and refractive indices for each aerosol's component using Akermann's model 0:

$$n_k^{RH}(r) = \frac{N_{tot}\cdot\mu_k}{(2\pi)^{1/2}\cdot r\cdot\ln\sigma_k}\cdot\exp\left[\frac{-\ln\left(\frac{r}{r_k^{RH}}\right)}{2\cdot\ln^2\sigma_k}\right] \tag{29}$$

$$m_k^{RH} = m_a + \left(m_k^0 - m_a\right)\cdot\left(\frac{r_k^0}{r_k^{RH}}\right)^3 \tag{30}$$

where *k* is referring to the soluble(s), insoluble (i) and carbonic components (c), the indices "*0*" refers to the values of microphysical parameters at *0* relative humidity and the "*RH*" indices refers to the corresponding value at relative humidity *RH*.

These will be input in Mie model for determination of theoretical extinction and backscatter coefficients $\beta_t(Z)$ and theoretical Lidar ratio 0.

$$LR_a^{RH} = \frac{\sum_{k=s,i,c} Q_{ext,k}^{RH}\left(r, m_k^{RH}, \lambda\right)\pi r^2 n_k^{RH}(r)dr}{\sum_{k=s,i,c} Q_{bksc,k}^{RH}\left(r, m_k^{RH}, \lambda\right)\pi r^2 n_k^{RH}(r)dr} = \frac{\sum_{k=s,i,c}\alpha_k^{RH}}{\sum_{k=s,i,c}\beta_k^{RH}} \tag{31}$$

Molecular backscattering coefficients calculated by the atmospheric model, the Lidar signal and $\beta_a(Z_C)$ in the calibration point Z_c are used by Fernald-Klett algorithm to calculate the experimental backscattering coefficient $\beta_e(Z)$ according to eq. (18)

The control parameter μ_c will be varied until the difference between $\beta_t(Z)$ and $\beta_e(Z)$ is less then a threshold. At this point conclusion is that the hypothesis made for the aerosols components is correct and microphysical aerosols parameters like AOD, effective radius, total volume concentration, can be derived. Now we have the correct value for extinction and backscatter coefficients. For the next profile point the iteration will start with the controlling parameter determined.

The method we are using is a regularization one because implies it a regularization cycle for controlling parameter, μ_c until we are getting an theoretical profile of β_a almost equivalent to the measured one. This is a hybrid

method because on each iteration, for derivation of experimental β_a by Lidar inversion, we are using as input the theoretical value of the Lidar ratio LR_a obtained with Akermann and Mie model.

4. Results and discussion

In the following will be presented a dust intrusion episode, which was recorded on April 5th, 2006, during a Lidar measurements campaign. The phenomena were consistent with the prognosis of DREAM (The Dust REgional Atmospheric Model) developed by Dr. Slobodan Nickovic 0 and running at the Supercomputing Center in Barcelona.

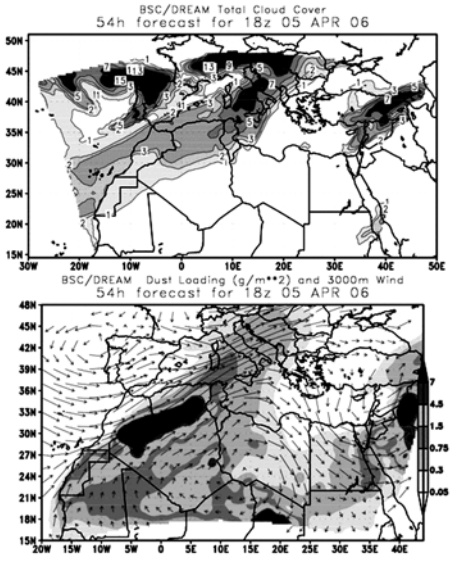

a

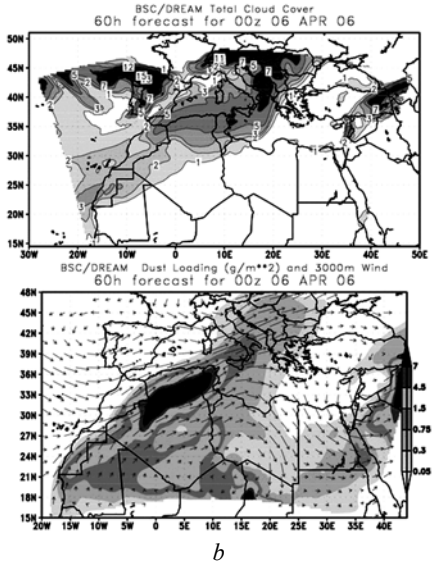

b

Fig. 4. DREAM forecast for April 5th 2006: 18 hours (a) and 24 hours (b) universal time [90].

The dust intrusion was forecast to reach Romanian teritory on April 5th around 12 hours local time. On Lidar signal (Bucharest area) it became visible right after the disapearence of the morning thermical inversion layer of the PBL which was suggested by the strong turbulence shown in RCS. The maximum intrusion was noticed around 16 hours. After that, due to the strong wind, the dust was dispersed and the phenomena decreased in intensity after sunset. Conform to the DREAM forecast 0, the dust came from Iberic Peninsula and was carried out by the air masses coming from south-west over Europe to Romanian teritory.

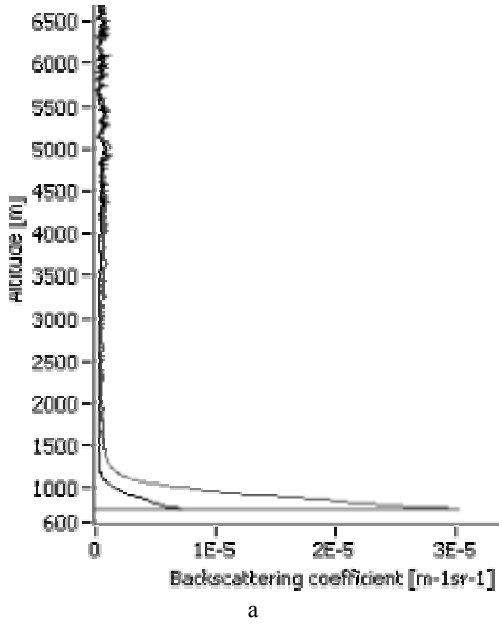

a

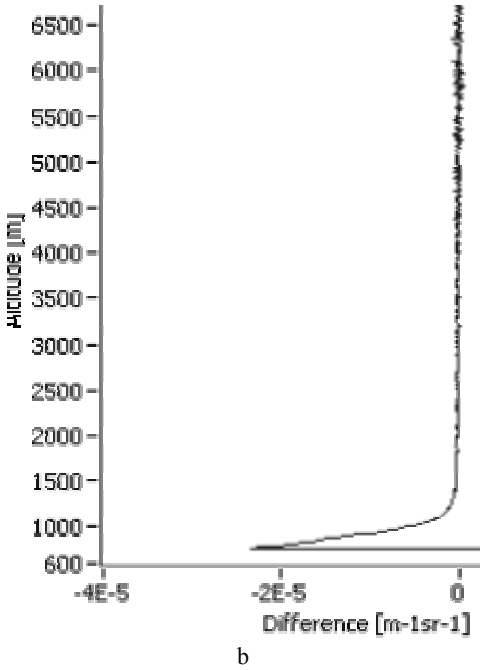

b

Fig. 5. The retrieval of backscattering coefficient using Fernald-Klett (gray line) and LiSA (black line) algorithm on April 4th 2006 (a) and difference between the 2 methods (b).

In the following figures some examples of processed Lidar data recorded during this event are presented. In Fig. 5 a comparative backscattering coefficient profile recorded on the previous day (April 4th) is presented. Dust intrusion

is visible in Fig. 6 (before sunset) and Fig. 7 (after sunset). For the three examples, a 10 measurements average was used in order to calculate the backscattering coefficient profile by using both simple Fernald-Klett and LiSA data processing methods. Profiles without clouds were chosen for processing. In the Figs. 6b and 7b the difference between the 2 methods in deriving the backscattering coefficient is shown.

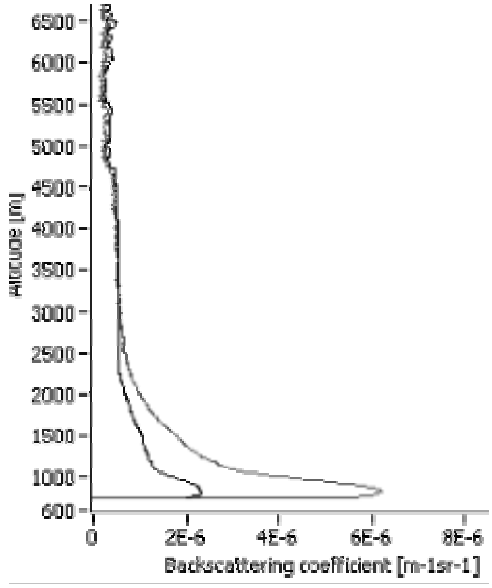

a

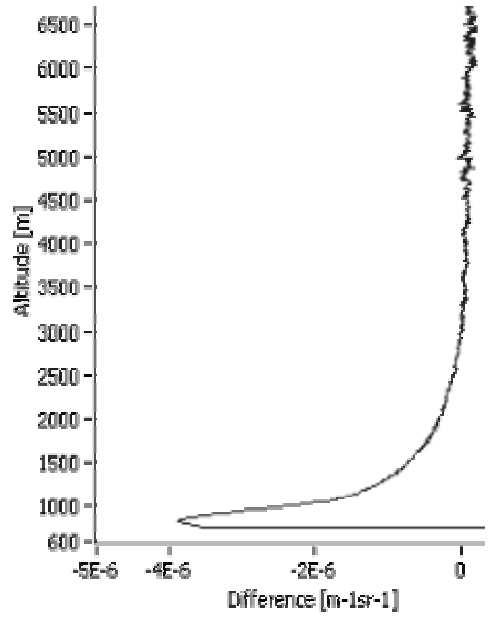

b

Fig. 6. The retrieval of backscattering coefficient using Fernald-Klett (gray line) and LiSA (black line) algorithm on April 5th 2006 (before sunset) (a) and difference between the 2 methods (b).

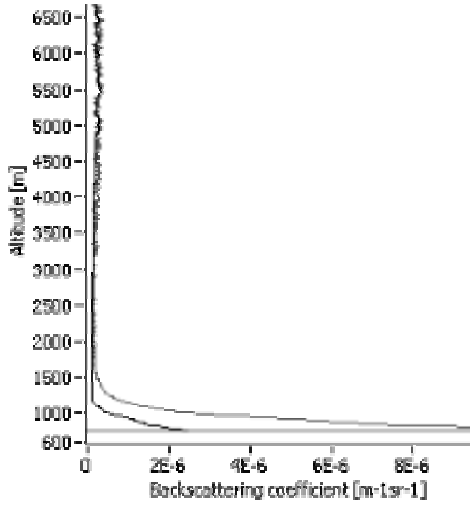

a

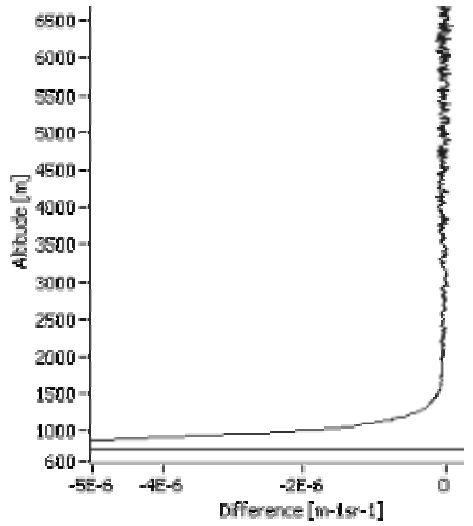

b

Fig. 7. The retrieval of backscattering coefficient using Fernald-Klett (gray line) and LiSA (black line) algorithm on April 5th 2006 (after sunset) (a) and difference between the 2 methods (b).

It can be noted first of all that, in case of normal atmosphere with a relatively constant humidity profile and without dust intrusion (Fig. 5) the 2 inversion methods provide similar results. This is due to the fact that the altitude variation of Lidar ratio is neglijible in this case, except for the lower part of the profile, inside PBL, where during the day a significant loading of pollutants is present. These pollutants come from traffic and industrial activities, have different microphysical properties due to their chemical composition and influence therefore the value of Lidar ratio. In the case of dust intrusion (Fig. 6 and 7), the presence of dust cloud between 4500 and 7000 m altitude determines an increase of soot particles mixing ratio μ_c and in consequence of the Lidar ratio. For that, the 2 inversion methods give different results in the mentioned altitude interval and also in the PBL (between 600 and 2000 m). As DREAM model forecasted, the

phenomena continues after the sunset but the atmospheric calm and PBL diurnal evolution favours the dispersion of the dust in the lower layers. This can be shown in Fig. 8b, where the Lidar ratio profile is uniform by comparison with the situation before sunset (Fig. 8a) and also in Fig. 9b, where the soot proportion is more constant then in Fig. 9a.

It must be noted that the average value of the Lidar ratio used in Fernald-Klett algorithm was 58 sr before sunset and 73 sr after sunset, those values being obtained for a minimum difference between the 2 inversion methods. Also, the soot proportion was 87% before sunset and 95% after sunset, which evidences once again a process of modification of atmospheric characteristics between the 2 time intervals in the sense of increased pollution level.

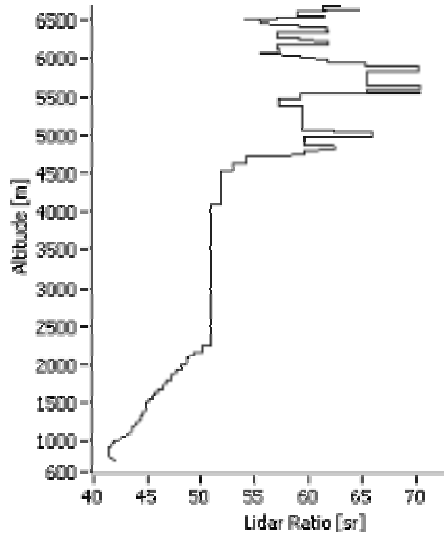

a

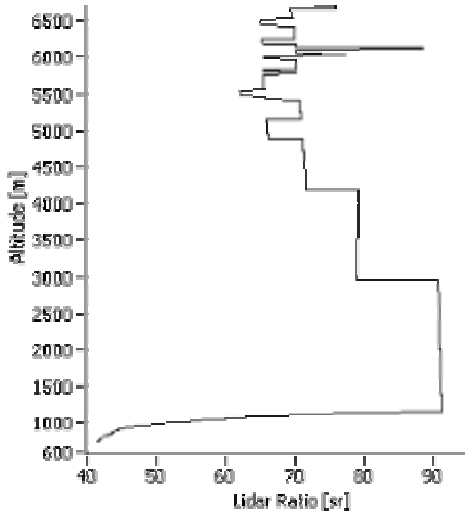

b

Fig. 8. Lidar ratio profile derived by LiSA on April 5th before sunset (a) and after sunset (b).

Another example which demonstrates the importance of considering a variable Lidar ratio as input parameter in inversion algorithm is the case of cloudy sky (Fig. 10 , 11a and 11b). Inside clouds the Lidar ratio has an important variation due to the cloud particles composition and their refractive index. Lidar ratio can not longer be considered constant with altitude. In the figures bellow only the profiles measured in the presence of cirrus clouds were considered and one can see that in this case the difference between the 2 methods become important. Inside a cloud, the dimension of hygroscopic aerosol increases (so that it becomes more "visible" in the 1064 nm sounding radiation then in 532 nm), the refractive index varies inducing a stronger scattering and weeker absorption of light. For this reason, clouds are "visible" directly in Lidar signal, unlike dust aerosols. The hygroscopic characteristics of cloud particles correspond to a incresing of soluble particles proportion and a decreasing of soot particles proportion, which is visible in Fig. 11b (soot, insoluble and soluble proportions are normalized).

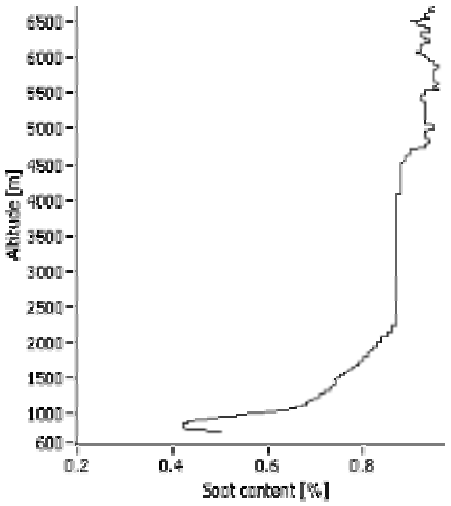

a

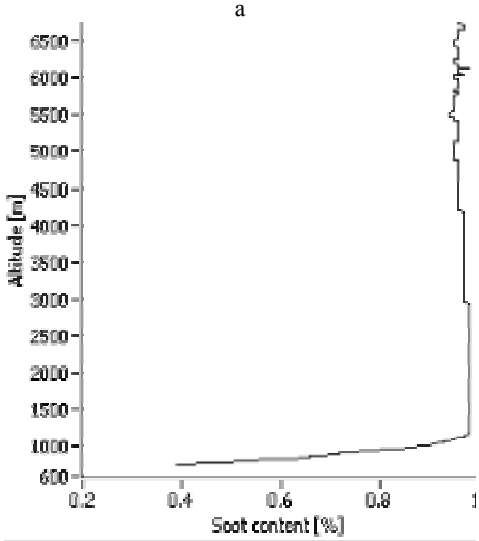

b

Fig. 9. Soot proprotion profile derived by LiSA on April 5th before sunset (a) and after sunset (b).

It must be noted although that, in elaborating LiSA algorithm, the multiple scattering was neglected, that's why the quantitative information reffering to cloud particles's optical properties must be carrefully analyzed.

Also, the calibration point must be properly chosen, above PBL and above the cloud, where the aerosol backscattering coefficient has a minimum value. This choice assures the convergence of the solution, which is not always evident, especially if both foreward and backward integration is used.

For the presented cases, the calibration point was choosed at 5500 m altitude, above the cloud, and a 87% soot proportion in that point was considered. This value was given by Ackermann [88] as the average value for continental urban troposphere. The relative humidity profile was extracted from NOAA database. For the dry values of effective radius and refractive index of every aerosol component the Ackermann hypothesis were used (these are based on numerous previous studies made by Whitby (1978) [91], Shettle (1979) [92], Bodhaine (1991) [93], Porter (1999) [94], Baron (2001) [95] and others [96-99]). With these considerations, the backscattering coefficient obtained in calibration point was $4.5e^{-7}$ $m^{-1}sr^{-1}$ for 1064 nm, respectively $1.16e^{-6}$ $m^{-1}sr^{-1}$ for 532nm, and the corresponding Lidar ratio was 51sr for 1064 nm, respectively 50 sr for 532 nm, those values being used as input in Fernald-Klett algorithm.

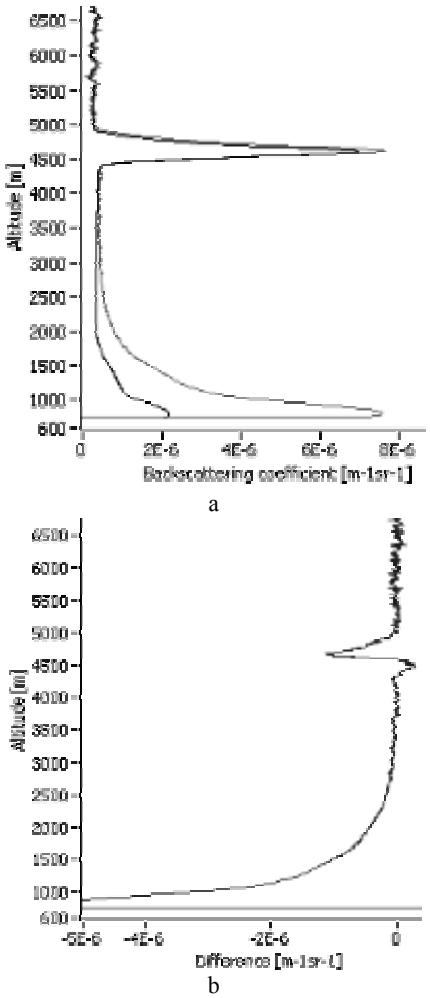

Fig. 10. The retrieval of backscattering coefficient using Fernald-Klett (gray line) and LiSA (black line) algorithm on April 5th 2006 (cloudy sky) (a) and difference between the 2 methods (b).

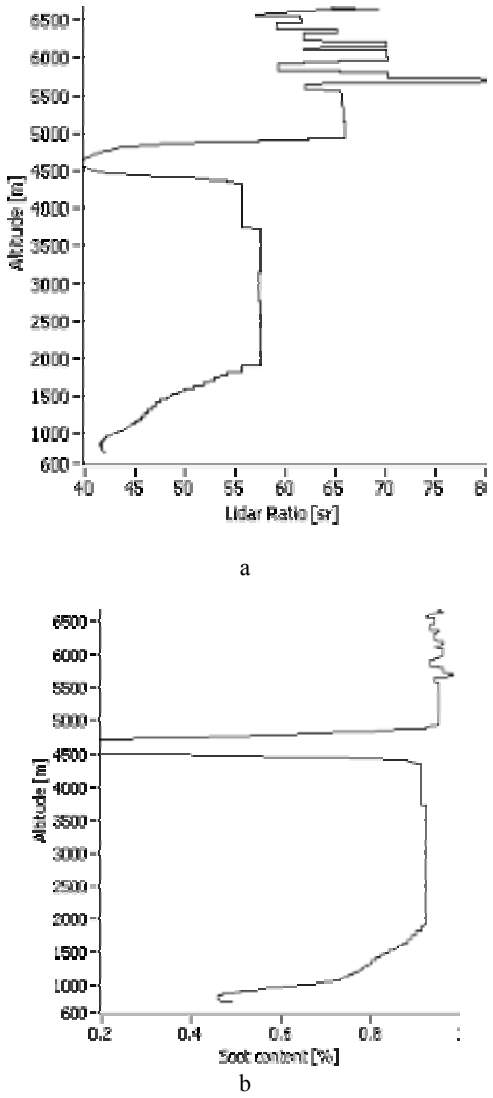

Fig. 11. Lidar ratio (a) and soot proportion profile (b) derived by LiSA on April 5th in case of cloudy sky.

5. Conclusions

Lidar systems can be very useful in environmental investigations, especially of the atmosphere, due to the large covered area and the real time response. The accuracy of obtained information is dependent of technical performances of the device and of sensibility of data processing method, which can be critical in some cases.

In the case of LiSA system (backscattering Lidar, only elastic Rayleigh and Mie scattered light), increased sensibility was obtained through minimization of relative signal $F(Z)/F(Z_\infty)$ experimental errors (performing system components, high operating stability) [100] and improvement of processing algorithm through combination of the Fernald-Klett solution with atmospheric model, Mie model and Ackermann model. This algorithm can be applied successfully to determine

the cloud and aerosol microphysics from elastic backscattering Lidar data.

In that sense, it must be noted that by considering a constant profile of Lidar ratio (as in Fernald-Klett algorithm), the errors in the retrieval of the backscattering coefficient are significant. Even if the value of the Lidar ratio is properly chose (for example, in our demonstration the same value of the Lidar ratio in the calibration point was used for both methods so that the differences are only due to vertical variations of aerosol's components proportions and their microphysics), the differences between the 2 methods are important in the PBL and inside the cloud. Also, without any complementary data, no aerosol microphysical parameter can be derived from elastic backscatter Lidar data. Nevertheless, the cloud base and height are well identified by both methods because only the optical characteristics are different and not the geometrical ones. This means that for extracting the altitude of cloud base and height the use of Fernald-Klett algorithm is sufficient, which consumes less computer resources [23]. To derive aerosol microphysical parameters and to improve the quantitative retrieval of optical parameters, the iterative algorithm or complementary measurements (Raman) must be used.

In any case, due to inherent assumptions made for the data inversion, the quantitative results must be carefully analyzed and data validation (using e.g. satellite data) must be done.

References

[1] E. H. Synge, Phil. Mag. and J. Sci. **9**(60), 1014 (1930).

[2] E. O. Hulbert, J. Opt. Soc. Am. **27**(11), 377 (1937).

[3] E. A. Johnson, R. C. Meyer, R. E. Hopkins, W. H. Mock, J. Opt. Soc. Amer. **29**(12), 512 (1939).

[4] L. Elterman, Geophys. Res. Papers no. 29, Air Force Cambridge Res. Center, 1954.

[5] S. S. Friedland, J. Katzenstein, M. R. Zatzick, J. Geophys. Res. **61**, 415–34 (1956).

[6] L. D. Smullin, G. Fiocco, Nature, **194**, 1267 (1962).

[7] G. Fiocco, L. D. Smullin, Nature, **199**(4900), 1275 (1963).

[8] B. R. Clemesha, G. S. Kent, R. W. H. Wright, Nature **209**(5019), 184 (1966).

[9] P. D. McCormick, S. K. Poultney, U. Van Wijk, C. O. Alley, R. T. Bettinger, J. A. Perschy, Nature **209** (5025), 798 (1966).

[10] W. C. Bain, M. C. W. Sandford, J. Atmos. Terrest. Phys. **28** (6/7), 543 (1966).

[11] H. Kölsch, P. Rairoux, J. P. Wolf, L. Wöste, Appl. Opt. **28**, 2052-2056 (1989).

[12] R. M. Measures, Krieger Publishing Company, Malabar, Florida, p. 237(1992).

[13] J. Bösenberg, et al., MPI Report, 348, Max-Planck-Institut für Meteorologie, Hamburg, Germany, 2003.

[14] V. Kovalev, V. Eichinger, Wiley Interscience Publ., New York, USA, 2004.

[15] V. Matthais et al., Applied Optics, **43**(4), 961 (2004).

[16] C. Bockmann et al., Applied Optics **43**(4), 977-989 (2004).

[17] G. Pappalardo et al., Applied Optics **43**(4), 5370 (2004).

[18] A. Papayannis et al., Atmospheric and Earth Sciences, 309-312, 21th International Laser Radar Conference, Quebec, Canada, 2002.

[19] C. Zerefos, P. Nastos, D. Balis, A. Papayannis, A. Kelepertsis, E. Kanellopoulou, D. Alexakis, C. Meleti, D. Nicolakis, P. Kandylis, K. Eleftheratos, W. Thomas, Advances in Space Physics, in press, 2005.

[20] D. N. Nicolae, C. Talianu, M. Ciobanu, V. Babin, SPIE, vol. 5227, p.472-479, 2002

[21] C. Radu, D. N. Nicolae, C. Talianu,, M. Ciobanu, V. Babin, M. Mustata, Proceedings of "International Conference on Physics TIM 03", 2003.

[22] Doina Nicoleta Nicolae, Camelia Talianu, Mircea Ciobanu, Vasile Babin, Cristian Radu, ESA Special Publication Sp-561, 2004, p.515-518.

[23] Camelia Talianu, Doina Nicoleta Nicolae, Mircea Ciobanu, Vasile Babin, Constantin P. Cristescu, ESA Special Publication Sp-561, 2004, p.255-258.

[24] R. Radvan, V. Coman, D. N. Nicolae, Proceedings of "Cultural Heritage Research: a Pan-European Challenge", Cracow, 2002

[25] Anca Nemuc, Doina Nicolae, Emil Carstea, Camelia Talianu, Proceedings of "7th ISTP - International Symposium on Tropospheric Profiling", Boulder, USA (to appear).

[26] Camelia Talianu, Doina Nicolae, Jeni Ciuciu, Proceedings of "International Symposium Environment and Industry – ECOIND" 2005, Bucharest.

[27] Camelia Talianu, Doina Nicolae, Jeni Ciuciu, Mircea Ciobanu, Vasile Babin, Cristian Radu, Proceedings of "Lidar Remote Sensing for Environmental Monitoring VI", 2005, San Diego, USA.

[28] L. Belegante, D. Nicolae, A. Nemuc, C. Talianu, E. Carstea, Proceedings of „Conference on Visibility, Aerosols, and Atmospheric Optics" Viena, 2006 (to appear).

[29] G. Mie, Ann. de Phys., Leipzig **25**, 377 (1908).

[30] C. W. Helstrom, Academic Press, New York, Math in Science and Engineering, 1976.

[31] M. Born, E. Wolf, Principles of Optics. Electromagnetic theory of propagation, interference and diffraction of light, Pergamon Press, New York, 1973.

[32] C. F. Bohren, D. R. Huffman, Absorption and Scattering of Light by Small Particles, Wiley, New York, 1983.

[33] M. I. Mishchenko, J. Opt. Soc. Am. A, **8**(6), 871-882 (1991).

[34] M. I. Mishchenko, L. D. Travis, J. Quant. Spectrosc. Radiat. Transfer **60**(3), 309-324 (1998).

[35] M. I. Mishchenko, J. W. Hovenier, L. D. Travis, Light Scattering by Nonspherical Particles. Theory, Measurements, and Applications, Academic Press,

San Diego, p. 152-157, 2000.
[36] S. Ştefan, Fizica Atmosferei, vremea şi clima, Editura Universităţii Bucureşti, 2004.
[37] ***, SAA Summary Report Atmospheric Resources, The University of Tennessee, http://sunsite.utk.edu/.
[38] V. Ramanathan, P. J. Crutzen, J. T. Kiehl, D. Rosenfeld, Science, **294**, 2119-212 (2001).
[39] R. J. Charlson, J. Heintzenberg, (Eds.), J. Vol. Environmental Sciences Research Report 17. 1995, New-York: John Wiley & Sons, Ltd.
[40] M. Kulmala, L. Pirjola, J. Makela, Nature **404**, 66-69 (2000).
[41] W. C. Hinds, Aerosol technology, John Wiley & Sons, New York, 1999.
[42] M. Kulmala, H. Vehkamaki, T. Petaja, M. dal Maso, A. Lauri, V.-M. Kerminen, W. Birmili, P. H. McMurry, J. Aerosol Sci., accepted, 2003.
[43] R. Jaenicke, P. V. Hobbs, Academic Press, San Diego, 1-31, 1993.
[44] G. Buzorius, K. Hameri, J. Pekkanen, M. Kulmala, Atmos. Env. **33**, 553-565 (1999).
[45] L. Morawska, S. Thomas, M. Jamriska, G. Johnson, Atmos. Environ. **33**, 4401- 4411 (1999).
[46] P. L. Jenkins, T. J. Phillips, J. M. Mulberg, S. P. Hui, Atmos. Environ. **26A**, 2141-2148 (1992).
[47] P. A. Baron, K. Willeke, Aerosol measurements: principles, techniques and applications, John Wiley & Sons, 2001.
[48] R. W. Bouble, D. L. Fox, D. Bruce Turner, A. C. Stern, Fundamentals of Air Pollution, Academic Press, San Diego, 1994.
[49] J. F. Slater, New Hampshire Ph.D. Thesis Earth Science Department University of New Hampshire, 2001.
[50] T. Vesala, M. Kulmala, R. Rudolf, A. Vartala, P. A. Wagner, J. Aerosol Sci. **28**(4), 565-598 (1997).
[51] W. Birmili, A. Wiedensohler, J. Heintzenberg, K. Lehmann, J. Geophys. Res. 106, D23, 32,005/32,018, 2001.
[52] C. Junge, J. Geophys. Res. **77**, 5183-5200 (1972).
[53] I. K. Koponen, Report Series In Aerosol Science 63, 2003.
[54] P. Monkkonen, R. Uma, D. Srinivasan, I. K. Koponen, K. E. Lehtinen, K. Hameri, R. Suresh, V. P. Sharma, M. Kulmala, Atmos. Env, 2003.
[55] T. Vesala, J. Haataja, P. Aalto, N. Altimir, G. Buzorius, E. Garam, K. Hameri, H. Ilvesniemi, V. Jokinen, P. Keronen, T. Lahti, T. Markkanen, J. M. Makela, E. Nikinmaa, S. Palmroth, L. Palva, T. Pohja, J. Pumpanen, U. Rannik, E. Siia, H. Ylitalo, P. Hari, M. Kulmala, Mass & Momentum Transfer, **4**, 17-35 (1998).
[56] J. M. Makela, P. Aalto, V. Jokinen, T. Pohja, A. Nissinen, S. Palmroth, T. Markkanen, K. Seitsonen, H. Lihavainen, M. Kulmala, Geophys. Res. Lett. **24**, 1219-1222 (1997).
[57] M. Kulmala, K. Hameri, P. P. Aalto, J. Makela, L. Pirjola, E. D. Nilsson, G. Buzorius, U. Rannik, M. Dal Maso, W. Seidl, T. Homan, R. Janson, H.-C. Hansson, Y. Viisanen, A. Laaksonen, C. O'Dowd, Tellus, **53B**, 324-343 (2001).
[58] J. W. Fitzgerald, Atmos. Environ. **29**, 837-849 (1991).
[59] C. D. O'Dowd, M. H. Smith, I. E. Consterdine, J. A. Lowe, Atmos. Environ. **31**, 73-80 (1997).
[60] J. Heintzenberg, D. C. Covert, R. Van Dingenen, Tellus, Ser. B, **48**, 197-212 (2000).
[61] J. P. Shi, A. A. Khan, R. M. Harrison, Sci. Total Environ. **235**, 51-64 (1999).
[62] W. A. Hoppel, G. M. Frick, R. E. Larson, Geophys. Res. Lett. **13**, 125-128 (1986).
[63] T. L. Jensen, S. M. Kreidenweis, Y. Kim, H. Sievering, A. Pszenny, J. Geophys. Res. **101**, 4455-4467 (1996).
[64] F. J. Brechtel, S. M. Kreidenweis, H. B. Swan, J. Geophysical Res. **103**, 16351-16367 (1998).
[65] M. Hess, P. Koepke, I. Schult, Bull. Amer. Meteor. Soc. **79**, 831-844 (1998).
[66] S. E. Schwartz, J. Aerosol Sci. **27**, 359–382 (1996).
[67] S. Pandis, A. Wexler, J. Seinfeld, 1995, J. Phys. Chem. **99**, 9646-9659 (1995).
[68] M. Andreae, P. Crutzen, Science **276**, 1052-1057 (1997).
[69] A. M. Thompson, J. Witte, R. Hudson, H. Guo, J. Herman, M. Fujiwara, Science **291**, 2128-2132 (2001).
[70] J. M. Prospero, P. Ginoux, O. Torres, S. E. Nicholson, T. E. Gill, Rev. Geophys. **40**, 1002 doi:10.1029/2000RG000095, (2002).
[71] F. A. Ackermann, H. Chung, J. Appl. Meteor. **31**, 223-236 (1992).
[72] J. H. Seinfeld, S. N. Pandis, J. Wiley and Sons, New York, USA, 1998.
[73] J. T. Houghton, W. Ding, D. J. Griggs, M. Noguer, P. J. van der Linden, Xiaosu, IPCC, Cambridge University Press, U.K, 2001.
[74] J. Ackermann, Appl. Opt. **36**, 5134-5143 (1998).
[75] Rayleigh, Lord, Philos. Mag., vol. 41, 107-120, 274-279 (reprinted În Sci. Papers **I**(8), 1869-1881, Dover, New York, 1964.
[76] D. N. Nicolae, C. Talianu, M. Ciobanu, V. Babin, G. J. Ciuciu, Proceedings of "Scientific reunion of the special program of the Alexander von Humboldt Foundation concerning the reconstruction of the South Eastern Europe AvH05", p. 79-82, ISBN 973-625-204-3, 2005.
[77] F. G. Fernald, B. M. Herman, J. A. Reagan, J. Appl. Meteorol. **11**, 482–489 (1972).
[78] J. D. Klett, Appl. Opt. **20**, 211–220 (1981).
[79] V. A. Kovalev, H. Mossmuller, Appl. Opt. **33**, 6499-6507 (1994).
[80] I. Balin, Thèse no 2975, Ecole Polytechnique Fédérale de Lausanne, 2004.
[81] J. A. Reagan, et al., J. Appl. Met.**16**, 911-928 (1977).
[82] P. Piironen, E. W. Eloranta, Opt. Lett. **19**, 234-236 (1994).
[83] I. Mattis, et al., Geophys.Res. Let. **29**, 1306 (2002).
[84] D. N. Nicolae, C. Talianu, J. Ciuciu, M. Ciobanu, V. Babin, J. Optoelectron. Adv. Mater. 2006, **8**(1),

238-242 (2006).
[85] D. N. Nicolae, C. Talianu, C. Ionescu, M.Ciobanu, J. Ciuciu, Proceedings SPIE 2005 (to appear).
[86] D. N. Nicolae, C. Talianu, C. P. Cristescu, Scientific Bulletin Journal of "Politehnica" University of Bucharest, A Serie **67**, 67-76 (2005).
[87] C. Talianu, D. N. Nicolae, J. Ciuciu, A. Nemuc, E. Carstea, L. Belegante, M. Ciobanu, Proceedings of "6 th International Conference SCEE -Scientific Computer in Electrical Engineering", Sinaia, Romania, 2006 (to appear).
[88] J. Ackermann, Journal of Atmospheric and Oceanic Technology, **15**(4), 1043-1050 (1997).
[89] S. Nickovic, A. Papadopoulos, O. Kakaliagou, G. Kallos, J. Geophys. Res. **106**, 18113-18129 (2001).
[90] http://www.bsc.es/projects/earthscience/DREAM/.
[91] K. T. Whitby, Atmos. Environ. **12**, 135-159 (1978).
[92] E. P. Shettle, R. W. Fenn, Air Force Geophysics Laboratory Environmental Research Papers 676, AFGL-TR79-0214, pp. 94, 1979.
[93] B. A. Bodhaine, N. C. Ahlquist, R. C. Schnell, Atmos. Env. **25A**:2267-2276 (1991).
[94] J. N. Porter, A. D. Clarke, http://www.soest.hawaii.edu, University of Hawaii, Honolulu, 1999.
[95] P. A. Baron, K. Willeke, Aerosol measurements: principles, techniques and applications, it John Wiley & Sons, 2001.
[96] T. Takamura, Y. Sasano, T. Hayasaka, Appl. Opt. **33**, 7132-7140 (1994).
[97] A. Waggoner, N. C. Ahlquist, R. J. Charlson, Appl. Opt., **11**, 2886-2889 (1972).
[98] J. D. Spinhirne, J. A. Reagan, B. M. Herman, J. Appl. Meteor. **19**, 426-438 (1980).
[99] J. M. Rosen, R. G. Pinnick, D. M. Garvey, J. Geophys. Res., **102**, 6017-6024 (1997).
[100] C. P. Cristescu, C. Talianu, D. N. Nicolae, M. Ciobanu, V. Babin, SPIE 5581-89, p. 701-711 (2004).

*Corresponding author: nnicol@inoe.inoe.ro